

Magneto-transport Signatures of a Magnetic Gap in Hybrid Topological Insulator-Ferromagnetic Insulator Heterostructure Devices

A. Kandala, A. Richardella, D. W. Rench, D. M. Zhang,* T. C. Flanagan, and N. Samarth[†]

Department of Physics and Materials Research Institute,

The Pennsylvania State University, University Park, PA 16802, USA

(Dated: December 7, 2012)

Abstract

We develop hybrid ferromagnetic insulator (GdN)/topological insulator (Bi_2Se_3) heterostructure devices to probe the effects of broken time reversal symmetry on electrical transport in the surface states of a three dimensional topological insulator. Low temperature ($0.28 \text{ K} \leq T \leq 30 \text{ K}$) measurements of electrical transport in laterally patterned devices show that interfacing Bi_2Se_3 with ferromagnetic GdN yields distinctive signatures in the quantum corrections to the longitudinal magnetoconductance, clearly differing from the standard weak anti-localization seen in control channels of Bi_2Se_3 . The absence of electrical transport in the insulating ferromagnetic GdN overlayer allows us to attribute these signatures to contributions from surface state transport in Bi_2Se_3 . We show that the observations are consistent with the opening of a magnetic gap in the surface state spectrum due to broken time-reversal symmetry.

Combining three dimensional (3D) topological insulators (TIs) with magnetism is of great current interest because of the unique effects predicted when the time reversal protected topological surface states are modified by symmetry breaking magnetic perturbations [1]. The resulting phenomena are as varied as the quantum anomalous Hall effect[2], the topological magneto-electric effect[3] and magnetic monopoles[4] among others. Experiments aimed at observing such phenomena have primarily focused on magnetically doped TIs[5–9]. In such materials, broken time-reversal symmetry leads to changes in the symmetry class of quantum corrections to transport [5, 6, 9], a hedgehog spin texture accompanied by a quenched Berry phase[8] and promising signatures of an emerging quantum anomalous Hall effect[7]. Complementary to the direct magnetic doping of TIs, several theoretical schemes have also proposed explorations of a different sample geometry wherein a patterned insulating ferromagnet (FM) is interfaced with a TI[10–15]. When the magnetic easy axis of the FM overlayer is out-of-plane, a gap opens in the surface states of the vicinal TI and this massive Dirac Hamiltonian should lead to chiral 1D edge states along FM domain walls where the mass changes sign. If the easy axis of the FM lies in-plane, no gap is expected to first order but the moment can be levered out-of-plane by an external field, thereby opening or closing a gap. More recently, theoretical calculations[16] have demonstrated that hexagonal warping effects can lead to a gap, even with an in-plane FM. Patterned FM overlayers could also be used to manipulate Klein tunneling in the Dirac surface states[10] and to create tunnel barriers in the surface state via proximity-induced exchange fields[11]. Such FM/TI heterostructure schemes have a clear advantage for electrical transport experiments: any unusual transport phenomena resulting from interfacing a TI with a FM can clearly be identified with surface states even if the chemical potential is large enough to allow for parallel bulk transport. In this *Letter*, we demonstrate an essential step towards such “magnetic gating” proposals by creating hybrid electrical transport devices wherein we interface an insulating FM (GdN) with a TI (Bi_2Se_3). By studying the quantum corrections to the magneto-resistance (MR) in patterned transport devices, we reveal the effect of broken time-reversal symmetry on the surface state and show that the data are consistent with the predicted opening of a magnetic gap.

GdN is an insulating FM of interest in the context of low temperature spintronic devices, particularly since it can be deposited by reactive sputtering at ambient temperature[17, 18]. This is of prime importance in studies of magnetic exchange coupling effects, as it minimizes

thermal diffusion of magnetic species. Changing the nitrogen composition allows access to metallic[19, 20], semiconducting[21] and insulating[18] regimes, opening possibilities for its use as a spin-injector and detector, a spin-filter[22] or a ferromagnetic gate in novel spintronic devices. The semiconducting and insulating states display a maximum ferromagnetic Curie temperature $T_C \sim 65 - 70$ K[18, 20, 21], while more conducting N-deficient forms can have T_C well above 100 K[18, 20].

Bi_2Se_3 thin films were grown by molecular beam epitaxy (MBE) on InP (111)A substrates under typical growth conditions described elsewhere[23]. Following a brief exposure to ambient atmosphere, the samples were transferred to a Kurt Lesker CMS-18 system; after an *in-situ* Ar^+ surface clean, GdN was deposited on the Bi_2Se_3 films by reactive rf sputtering of Gd in an $\text{Ar}:\text{N}_2$ environment at ambient temperature. The GdN films were deposited at a rate of ~ 0.1 Å/sec, with a sputtering power of 4.93 W/cm², in a 15% $\text{N}_2:\text{Ar}$ gas environment at 5 mTorr pressure, with a source to substrate distance of 20 cm. The base pressure in the chamber prior to sputtering was $\sim 4 \times 10^{-7}$ Torr. The lack of ultra high vacuum is probably responsible for the lower T_C of our films. Since GdN oxidizes instantly on exposure to atmosphere, the films were capped *in-situ* with ~ 60 nm of Au deposited by dc sputtering.

The structural and magnetic characterization of the heterostructures is shown in Fig. 1. We used cross-sectional high resolution transmission electron microscopy (HRTEM) to study the nature of the interface. The phase contrast image of Fig. 1(a) reveals a polycrystalline GdN layer on top of a single crystal thin film of Bi_2Se_3 . The selected area diffraction (SAD) pattern (Fig. 1(b)) taken over the Bi_2Se_3 region shows the diffraction pattern of the InP substrate and additional spots consistent with Bi_2Se_3 single crystal grown epitaxially along the $\langle 111 \rangle$ direction of InP. A fast Fourier transform (FFT) from the GdN region confirms its polycrystalline nature (Fig. 1(c)). No additional layer that could indicate an interfacial reaction is discernible. X-ray energy dispersive spectroscopy (EDS) line profile measurements were carried out in scanning TEM (STEM) mode to study the elemental distribution along the growth direction of the film stack. Figure 1(d) is a bright field image in STEM mode with the red line and the arrow indicating the line profile position and scan direction. Thirty EDS spectra were collected with a step size of 1.9 nm and a nominal probe size of ~ 2 nm. The line profile is plotted in Fig. 1(e). Each data point was obtained by integrating the K_α and K_β lines without a standard for calibration; and hence the results are qualitative.

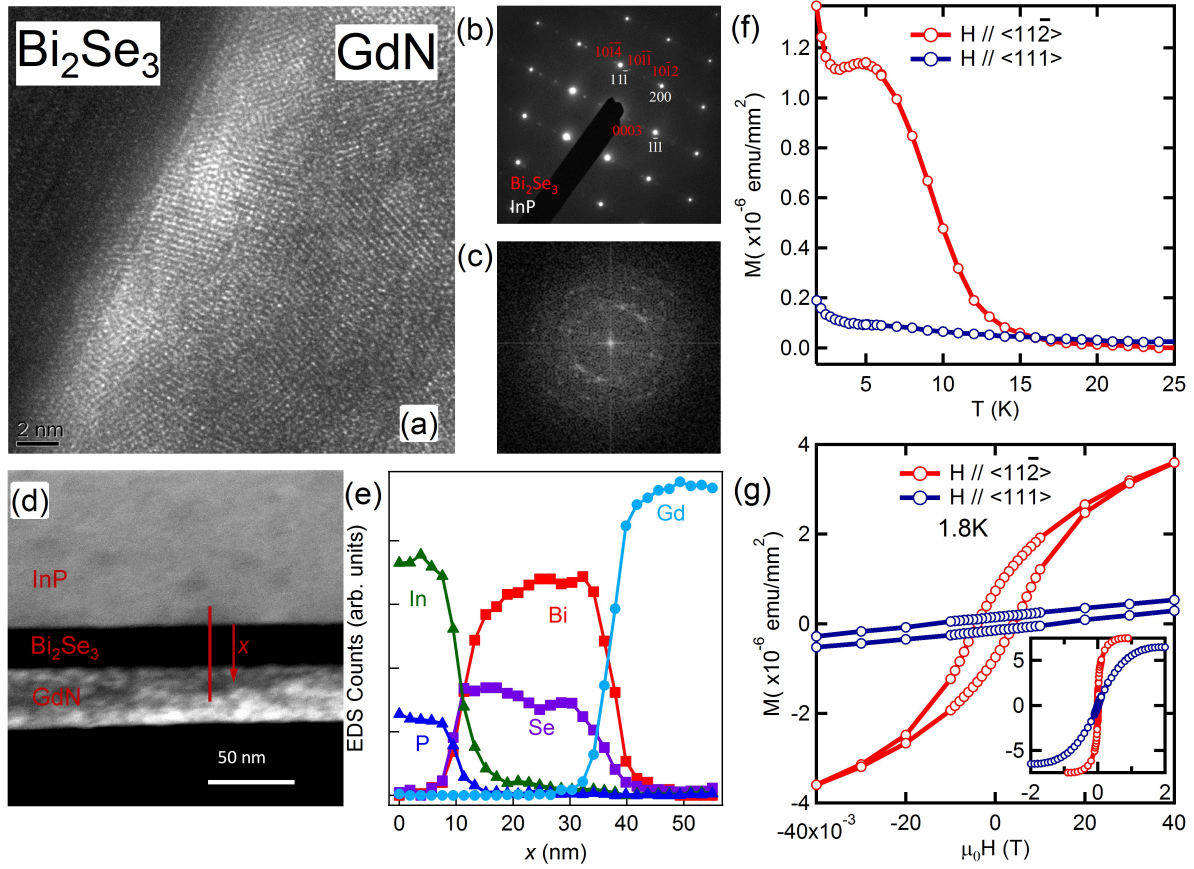


FIG. 1: (Color online) (a) HRTEM image of the heterostructure reveals a polycrystalline GdN thin film on a single crystal thin film of Bi_2Se_3 with no discernible interfacial layer. (b) SAD pattern depicts spots associated with the InP substrate and Bi_2Se_3 growing along the $\langle 111 \rangle$ direction. (c) FFT from the GdN region confirms its polycrystallinity. (d) Bright field image of the heterostructure. The red line and the arrow indicate the extent of the EDS line scan and scan direction respectively. (e) EDS line profile plot depicts the elemental distribution along the growth direction. (f) M vs T measurements of the $\text{Bi}_2\text{Se}_3/\text{GdN}$ heterostructure reveal $T_C \sim 13$ K. (g) M vs $\mu_0 H$ measurements at 1.8 K along the $\langle 11\bar{2} \rangle$ and $\langle 111 \rangle$ directions display hysteresis, and confirm that the easy axis is in-plane. Inset: M vs $\mu_0 H$ curves over a 2 T field range.

Nevertheless, the elemental distribution is consistent with the film stack and shows relatively sharp interfaces. Magnetization measurements in a superconducting quantum interference device (SQUID) magnetometer then confirmed the ferromagnetism in the heterostructures. Measurements were taken along both in-plane and perpendicular-to-plane directions in a 5

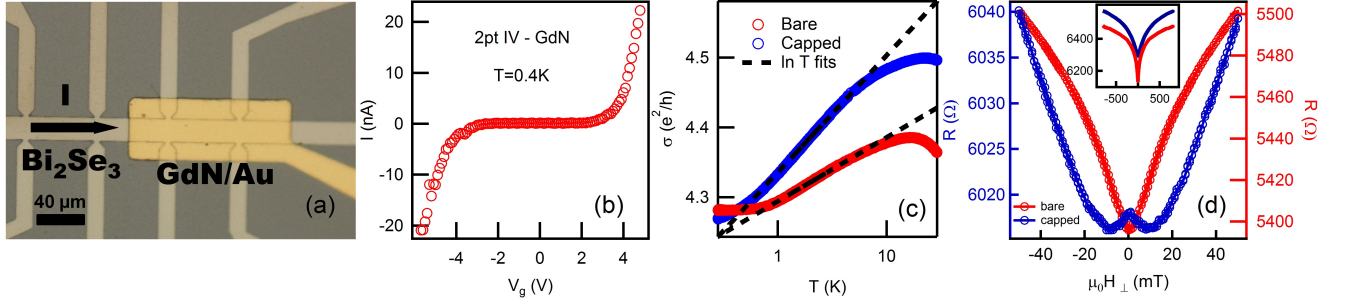


FIG. 2: (Color online) (a) Optical microscope image of a typical device depicts a Hall bar of Bi_2Se_3 with a bare channel and a channel capped with GdN/Au , enabling comparison of magnetotransport. (b) 2 probe $I - V$ curve of the $\text{Bi}_2\text{Se}_3/\text{GdN}/\text{Au}$ structure displays a strong non-linearity confirming the highly insulating nature of the GdN . (c) Temperature dependence of the 2D conductivity (σ) for the bare (red) and capped (blue) channels for $T \leq 30$ K is depicted in a semilog plot. Curves are offset for clarity. Dotted lines are fits to $\sigma \propto \ln T$. (d) MR at $T = 400$ mK over a 50 mT field range from capped (blue) and bare (red) channels. While the bare region shows a cusp-like positive MR typical of WAL, the region capped with ferromagnetic GdN has a superimposed negative MR. Inset: expanded view of MR over a 1 T field range reveals similar WAL at high fields for both capped and bare channels.

mT measuring field after a 0.9 T field cool. The temperature dependence of the magnetization M reveals the T_C to be around 13 K, obtained by extrapolating the line of steepest slope of the curve (Fig. 1(d)). The hysteresis loops in the M v/s $\mu_0 H$ plots (Fig. 1(e)) reveal the easy axis to lie in-plane.

We measured magnetotransport in Hall bar devices of an 8 nm thick Bi_2Se_3 thin film, patterned into multiple channels of dimension $20 \mu\text{m} \times 60 \mu\text{m}$ by standard photolithography and wet etching ($\text{K}_2\text{Cr}_2\text{O}_7:\text{HBr}:\text{DI}$). The ferromagnetic GdN/Au gate electrode is then defined over one of the channels by another step of photolithography, sputtering and a lift-off process. The sputtering conditions were identical to those employed for the magnetic characterization. Figure 2(a) is an image of a typical device showing channels of bare Bi_2Se_3 and ones covered with GdN . This enables a comparison of the magneto-transport properties of the Bi_2Se_3 film in both regions to see the effects of the insulating ferromagnetic layer. Transport measurements were carried out in a ^3He cryostat (operating temperature range 300 mK–30 K) with a superconducting vector magnet with a maximum full sphere

field of 1 T. Two probe measurements through the Au-GdN-Bi₂Se₃ heterostructure show a highly non-linear $I - V$ curve at 400 mK (Fig. 2(b)) confirming the insulating nature of the GdN. The asymmetry is indicative of two different Schottky barriers, one each at the Au/GdN and GdN/Bi₂Se₃ interfaces. This verifies that there are no contributions to transport from currents through the ferromagnet. The temperature dependence of the two dimensional (2D) sheet conductance (σ) of the bare and capped channels (Fig. 2(c)) shows a down-turn that follows a $\sigma \sim \ln(T)$ behavior consistent with electron-electron (e-e) interaction in two dimensions[24]. Hall measurements reveal a carrier density of $1.36 \times 10^{19} \text{ cm}^{-3}$ and $5.7 \times 10^{19} \text{ cm}^{-3}$ for the bare and capped channels. The larger carrier density observed in the capped channel may be due to interfacial defects. At 400 mK, both channels show a high-field positive MR attributed to weak anti-localization (WAL) due the large spin-orbit coupling in Bi₂Se₃ (inset, Fig. 2(d)). A closer look at the low-field regime reveals, however, a small negative MR below 10 mT in the capped channel, superimposed upon the WAL dip (Fig. 2(d)). No such feature is seen for the bare Bi₂Se₃ channel. This behavior was reproduced in a second device with a similar carrier density for the capped channel.

The temperature evolution of the change in MR of the capped channel is depicted in Fig. 3. The negative MR is very narrow at $T = 400 \text{ mK}$ but broadens continuously with increasing temperature and is seen to persist even at 30 K (the maximum operating temperature of the measurement system), well beyond the T_C of the GdN film. This indicates the importance of loose spins at the interface. The feature is always superimposed on top of a positive WAL and/or classical MR. These observations are emphasized in the line cuts in Fig. 3(b,c) of the raw MR at 5 K and 25 K. One possible interpretation would attribute the negative MR to spin disorder scattering from randomly oriented magnetic moments at zero-field, as observed in several dilute magnetic semiconductors[25]. The application of an external field aligns these moments, thereby reducing scattering and consequently, the resistance. In order to test this interpretation, we tilt the magnetic field towards the plane of the sample. The low-field MR is depicted for different tilt-angles in Fig. 3(d) and is seen to scale with the perpendicular component of the magnetic field (Fig. 3(e)). Such a scaling makes spin-scattering an unlikely origin for the negative MR and instead points towards weak localization phenomena (WL). Indeed, magnetically doped Bi₂Se₃ films [5, 9] and nanoribbons[6] have also displayed a similar negative MR that has been attributed to WL.

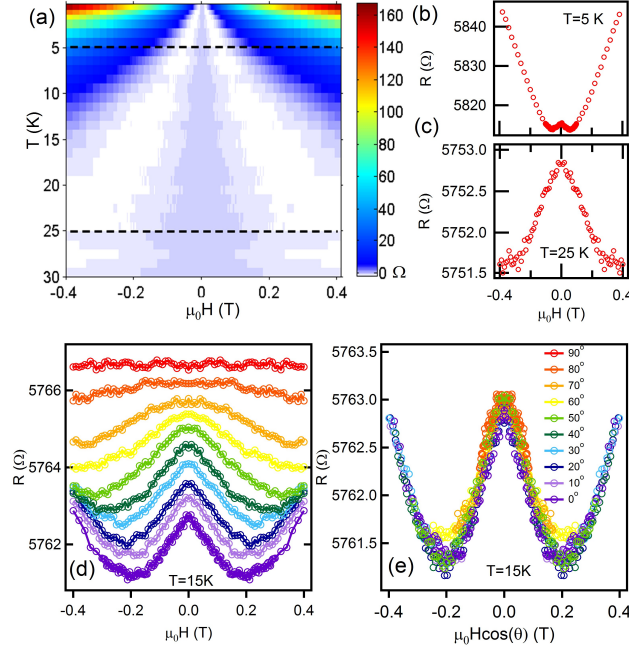


FIG. 3: (Color online) (a) MR ($\Delta R(H) = R(0) - R(H)$) of the GdN capped channel as a function of temperature T and magnetic field $\mu_0 H$. Panels (b) and (c) show the MR line cuts corresponding to the dotted lines at $T = 5$ K and $T = 25$ K. (d) Angular dependence of the MR of the capped channel, as the field is tilted from perpendicular-to-plane (violet) to in-plane (red), in 10° steps offset for clarity. (e) The MR of the capped channel scales with the perpendicular-to-plane component of the magnetic field H_\perp .

We present support for attributing the low field MR to WL by fitting the different quantum corrections to a modified[26] Hikami-Larkin-Nagaoka[27] (HLN) equation:

$$\Delta\sigma(B) = \sum_{i=0,1} \frac{\alpha_i e^2}{\pi h} \left[\Psi \left(\frac{l_B^2}{l_{\phi,i}^2} + \frac{1}{2} \right) - \ln \left(\frac{l_B^2}{l_{\phi,i}^2} \right) \right]. \quad (1)$$

In the above equation the α_i 's and $l_{\phi,i}$'s correspond to the pre-factors and coherence lengths respectively associated with WL and WAL, and l_B is the magnetic length. Although the fit employs four free parameters, fitting to the experimental data serves as a useful test of weak localization. Indeed, the fits work well in the temperature range below 15 K, as shown for the 4 K and 13 K data in Fig. 4(a). At higher T , increased relative contributions from the classical MC and/or the limited maximum field range precludes an effective fitting of the WAL. We also fit the regular HLN equation to the WAL data from the bare channel. A comparison of the different coherent lengths and pre-factors obtained is depicted in Fig. 4(b)

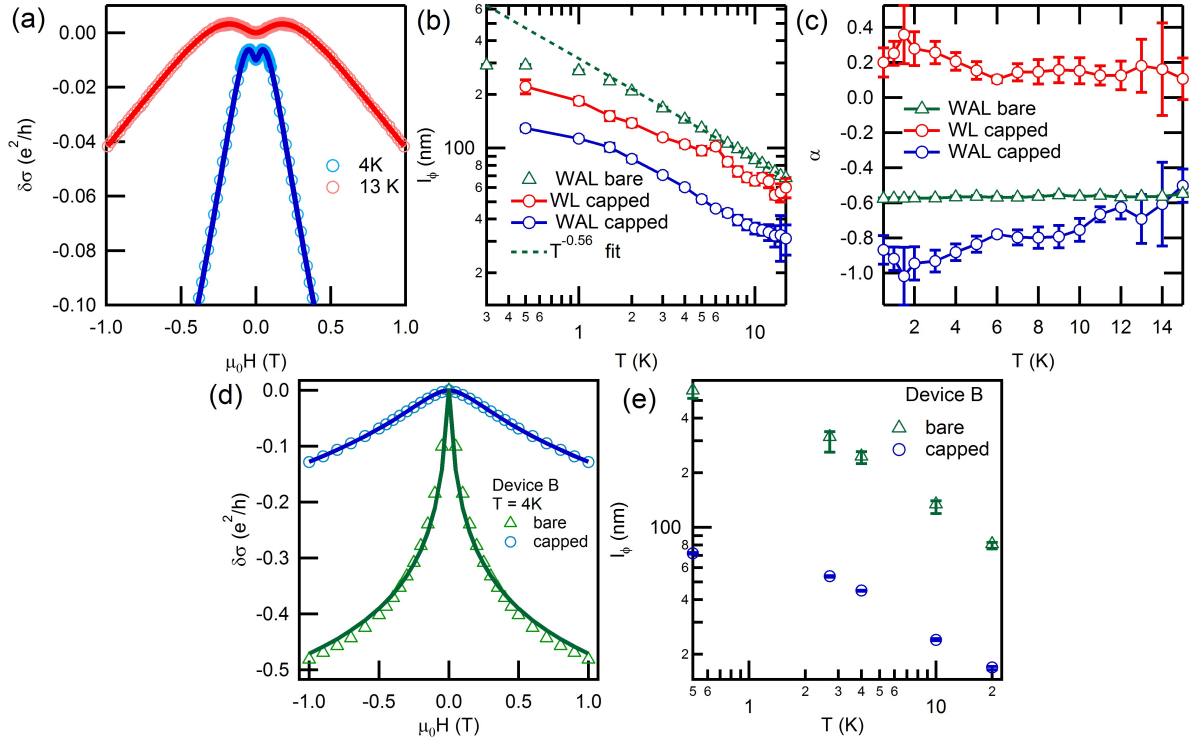


FIG. 4: (Color online) (a) Data (open circles) and modified HLN fits (bold lines) to the magnetoconductance of the capped channel at 4 K (blue) and 13 K (red). Curves are offset for clarity. (b) Temperature dependence of l_ϕ associated with WL in capped channel (red circles), WAL in capped channel (blue circles) and WAL in bare channel (green circles). The dashed green line is a $T^{-0.56}$ fit to the high-temperature dependence of l_ϕ of the bare channel, suggestive of e-e interaction as the dominant dephasing mechanism. (c) Temperature dependence of α associated with WL in capped channel (red circles), WAL in the capped channel (blue circles) and WAL in bare channel (green circles). Error bars are 95% confidence intervals of the fits. (d) Magnetoconductance in Device B shows a weakened WAL from the capped channel (blue circles) in comparison to the bare channel (red circles). (e) T dependence of l_ϕ of the bare (red) and capped (blue) channels in Device B.

and (c). The l_ϕ associated with the bare channel reaches a maximum of ~ 300 nm at 300 mK. The high temperature power law decay is suggestive of e-e interaction being the dominant dephasing mechanism. The l_ϕ associated with WL in the capped channel compare well with the bare channel, while those associated with WAL are seen to be significantly reduced. The α 's associated with both channels do not show a sharp temperature dependence over the discussed temperature range. Consistent with existing ideas, the α associated with WL is

seen to be positive and fluctuates in the range ~ 0.1 - 0.2 . However, the departure from the theoretical limit ($\alpha = 1$) may be attributed to significant magnetic scattering driving the system towards the unitary class. The magnetoconductance of a second device B with a significantly larger carrier density of $\sim 11 \times 10^{19} \text{ cm}^{-3}$ for the GdN capped channel revealed no signature of WL. Figure 4(d) however depicts the significantly weaker and broader WAL feature from the capped channel in comparison to the bare channel. Consequently, the l_ϕ associated with the capped channel in this device is also seen to be much shorter than the bare channel, possible due to increased defect scattering.

Intuitively, one would expect magnetic scattering to destroy any form of quantum interference. However, the opening of a sufficiently large gap in the surface state Dirac cone due to an out-of-plane magnetization at the surface is predicted[26] to yield a crossover from WAL to WL. The crossover is expected to be dependent on the ratio ($\Delta/2E_F$) of the gap size (Δ) to the Fermi energy with respect to the Dirac point (E_F). In the limit of small $\Delta/2E_F$, the MR is positive and dominated by WAL, crossing over to WL in the limit of large $\Delta/2E_F$ via an intermediate regime of parabolic, positive MR. Such phenomena are predicted to arise due to a competition between magnetic scattering and the opening of a gap in the surface state gap. Our data can therefore be interpreted as evidence for the opening of such a surface state gap due to broken time-reversal symmetry at the interface. The absence of a crossover to WL in device B may then be attributed to its larger carrier density and hence a larger E_F . The higher chemical potential also implies a larger bulk conductivity that overwhelms any surface related signal. The WAL component that is always seen in these devices may arise from the bulk or from the bottom surface state, both of which are unlikely to be affected by the magnetic atoms at the top interface.

Finally, we discuss the possible origins of the opening of a surface state gap in our devices. One possibility is that the application of a perpendicular magnetic field aligns the magnetization of the GdN out of plane. However, it is important to note that the WL is seen to persist beyond the T_C of the GdN, implying that the Dirac state gap also persists beyond T_C . Further, the values of α for the WL appear to be relatively temperature independent, implying that the size of the gap does not change much over the range of temperature studied. This raises the intriguing possibility of the development of an interfacial ferromagnetism with a much higher T_C than that of the GdN, that may be undetectable by conventional SQUID measurements. Indeed, recent mean field calculations predict a robust surface state

mediated ferromagnetism can arise due to RKKY interactions between magnetic atoms at the surface of a TI [28]. Given the large E_F in these samples, the origin of such an interfacial ferromagnetism is unclear but is consistent with signatures of a high T_C magnetically ordered state revealed in recent measurements of x-ray magnetic circular dichroism in Mn-Bi₂Se₃ thin films[8, 9].

In summary, we have developed a new class of hybrid TI heterostructure devices wherein the surface transport in the TI is influenced by an overgrown insulating ferromagnet. By designing Bi₂Se₃ devices that contain channels selectively capped or not capped with GdN, we carried out a direct comparison of magnetotransport properties with and without magnetic interactions. The crossover to WL in the capped channel is consistent with theoretical predictions that associate this behavior with the opening of a surface state gap. The development of these heterostructure devices opens up a broad range of opportunities for cleanly studying the influence of magnetism on electrical transport in the topological surface state.

This work was supported by DARPA (N66001-11-1-4110). We also acknowledge partial support from ONR (N00014-12-1-0117) and the Pennsylvania State University Materials Research Institute Nanofabrication Lab under the National Science Foundation Cooperative Agreement No. ECS-0335765.

* Current address: Center for Nanoscale Science and Technology, National Institute of Standards and Technology, Gaithersburg, MD 20899, USA.

† Electronic address: nsamarth@psu.edu

- [1] M. Z. Hasan and C. L. Kane, Rev. Mod. Phys. **82**, 3045 (2010).
- [2] R. Yu, W. Zhang, X. Dai, and Z. Fang, Science **329**, 61 (2010).
- [3] X.-L. Qi, T. L. Hughes, and S.-C. Zhang, Phys. Rev. B **78**, 195424 (2008).
- [4] X.-L. Qi, R. Li, J. Zang, and S.-C. Zhang, Science **323**, 1184 (2009).
- [5] M. Liu, J. Zhang, C.-Z. Chang, Z. Zhang, X. Feng, K. Li, K. He, L.-l. Wang, X. Chen, X. Dai, et al., Phys. Rev. Lett. **108**, 036805 (2012).
- [6] J. J. Cha, M. Claassen, D. Kong, S. S. Hong, K. J. Koski, X.-L. Qi, and Y. Cui, Nano Letters **12**, 4355 (2012).
- [7] J. Checkelsky, J. Ye, Y. Onose, Y. Iwasa, and Y. Tokura, Nat Phys **8**, 729 (2012).

- [8] S.-Y. Xu, M. Neupane, C. Liu, D. Zhang, A. Richardella, L. Andrew Wray, N. Alidoust, M. Leandersson, T. Balasubramanian, J. Sanchez-Barriga, et al., *Nat Phys* **8**, 616 (2012).
- [9] D. M. Zhang, A. Richardella, D. W. Rench, S.-Y. Xu, A. Kandala, T. C. Flanagan, H. Beidenkopf, A. L. Yeats, B. B. Buckley, P. V. Klimov, et al., *Phys. Rev. B* **86**, 205127 (2012).
- [10] J. Gao, W.-Q. Chen, X.-Y. Feng, X. Xie, and F.-C. Zhang, arXiv:0909.0378
- [11] S. Mondal, D. Sen, K. Sengupta, and R. Shankar, *Phys. Rev. Lett.* **104**, 046403 (2010).
- [12] T. Yokoyama, Y. Tanaka, and N. Nagaosa, *Phys. Rev. B* **81**, 121401 (2010).
- [13] I. Garate and M. Franz, *Phys. Rev. Lett.* **104**, 146802 (2010).
- [14] B. D. Kong, Y. G. Semenov, C. M. Krowne, and K. W. Kim, *Appl. Phys. Lett.* **98**, 243112 (2011).
- [15] Y. Tserkovnyak and D. Loss, *Phys. Rev. Lett.* **108**, 187201 (2012).
- [16] L. Oroszlány and A. Cortijo, *Phys. Rev. B* **86**, 195427 (2012).
- [17] J. Q. Xiao and C. L. Chien, *Phys. Rev. Lett.* **76**, 1727 (1996).
- [18] K. Senapati, T. Fix, M. E. Vickers, M. G. Blamire, and Z. H. Barber, *Phys. Rev. B* **83**, 014403 (2011).
- [19] P. Wachter and E. Kaldis, *Solid State Commun.* **34**, 241 (1980).
- [20] N. O. V. Plank, F. Natali, J. Galipaud, J. H. Richter, M. Simpson, H. J. Trodahl, and B. J. Ruck, *Appl. Phys. Lett.* **98**, 112503 (2011).
- [21] S. Granville, B. J. Ruck, F. Budde, A. Koo, D. J. Pringle, F. Kuchler, A. R. H. Preston, D. H. Housden, N. Lund, A. Bittar, et al., *Phys. Rev. B* **73**, 235335 (2006).
- [22] K. Senapati, M. Blamire, and Z. Barber, *Nat Mater* **10**, 849 (2011).
- [23] A. Richardella, D. M. Zhang, J. S. Lee, A. Koser, D. W. Rench, A. L. Yeats, B. B. Buckley, D. D. Awschalom, and N. Samarth, *Appl. Phys. Lett.* **97**, 262104 (2010).
- [24] J. Wang, A. M. DaSilva, C.-Z. Chang, K. He, J. K. Jain, N. Samarth, X.-C. Ma, Q.-K. Xue, and M. H. W. Chan, *Phys. Rev. B* **83**, 245438 (2011).
- [25] F. Matsukura, H. Ohno, A. Shen, and Y. Sugawara, *Phys. Rev. B* **57**, R2037 (1998).
- [26] H.-Z. Lu, J. Shi, and S.-Q. Shen, *Phys. Rev. Lett.* **107**, 076801 (2011).
- [27] S. Hikami, A. I. Larkin, and Y. Nagaoka, *Prog. Theor. Phys.* **63**, 707 (1980).
- [28] G. Rosenberg and M. Franz, *Phys. Rev. B* **85**, 195119 (2012).